A novel inhalable nanobody targeting IL-4Rα for the treatment of asthma

Min Zhu, MS, Linlin Ma, PhD, Peiyu Zhong, PhD, Jing Huang, MS, Junwei Gai, MS, Guanghui Li, MS, et al

GRAPHICAL ABSTRACT

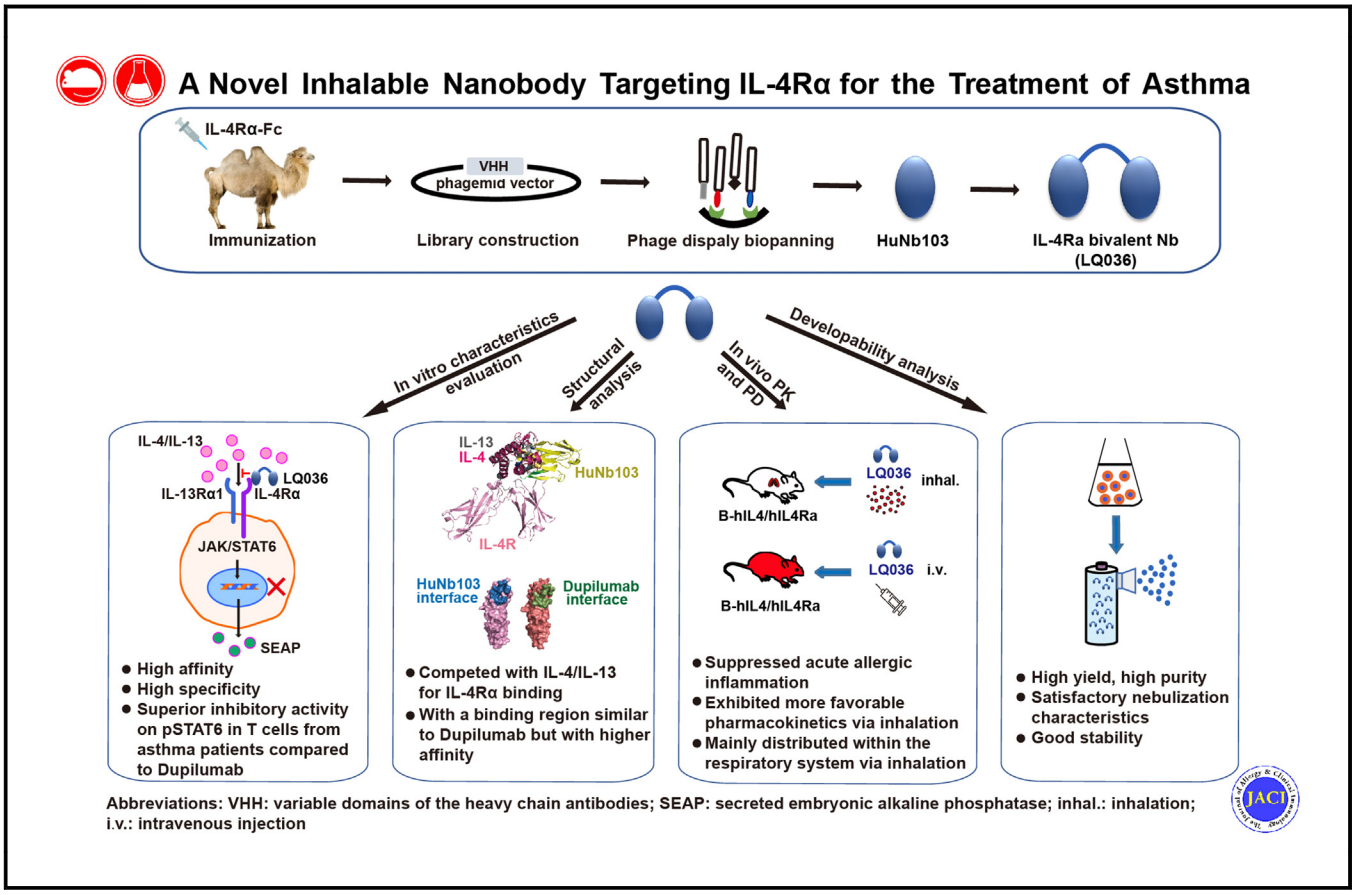

Capsule summary: The compelling efficacy, rapid onset, robust stability, and excellent safety profile of inhaled LQ036 underscore its potential as an innovative inhalable biologic therapy for asthma.

J Allergy Clin Immunol 2024;154:1008-21.

https://doi.org/10.1016/j.jaci.2024.05.027

A novel inhalable nanobody targeting IL-4Rα for the treatment of asthma

Min Zhu, MS,[a]* Linlin Ma, PhD,[b]* Peiyu Zhong, PhD,[c]* Jing Huang, MS,[a]* Junwei Gai, MS,[a] Guanghui Li, MS,[a] Yanfei Li, PhD,[b] Peng Qiao, MS,[a] Huaiyu Gu, BS,[a] Xiaofei Li, MS,[a] Yong Yin, PhD,[d,e,f] Lei Zhang, PhD,[d] Zhenzhen Deng, MS,[a] Baihe Sun, MS,[b] Zhihong Chen, PhD,[g]‡ Yu Ding, PhD,[c]‡ and Yakun Wan, PhD[a]‡ *Shanghai, China*

Background: Inhalable biologics represent a promising approach to improve the efficacy and safety of asthma treatment. Although several mAbs targeting IL-4 receptor α chain (IL-4Rα) have been approved or are undergoing clinical trials, the development of inhalable mAbs targeting IL-4Rα presents significant challenges.

Objective: Capitalizing on the distinctive advantages of nanobodies (Nbs) in maintaining efficacy during storage and administration, we sought to develop a novel inhalable IL-4Rα Nb for effectively treating asthma.

Methods: Three IL-4Rα immunized Nb libraries were used to generate specific and functional IL-4Rα Nbs. LQ036, a bivalent Nb comprising 2 HuNb103 units, was constructed with a high affinity and specificity for human IL-4Rα. The efficacy, pharmacokinetics, and safety of inhaled LQ036 were evaluated in B-hIL4/hIL4RA humanized mice.

Results: LQ036 inhibited secreted embryonic alkaline phosphatase reporter activity, inhibited TF-1 cell proliferation, and suppressed phosphorylated signal transducer and activator of transduction 6 in T cells from patients with asthma. Crystal structure analysis revealed a binding region similar to dupilumab but with higher affinity, leading to better efficacy in blocking the signaling pathway. HuNb103 competed with IL-4 and IL-13 for IL-4Rα binding. Additionally, LQ036 significantly inhibited ovalbumin-specific IgE levels in serum, CCL17 levels in bronchoalveolar lavage fluid, bronchial mucous cell hyperplasia, and airway goblet cell hyperplasia in B-hIL4/hIL4RA humanized mice. Inhaled LQ036 exhibited favorable pharmacokinetics, safety, and tissue distribution, with higher concentrations observed in the lungs and bronchi.

Conclusions: These findings from preclinical studies establish the safety and efficacy of inhaled LQ036, underscoring its potential as a pioneering inhalable biologic therapy for asthma. (J Allergy Clin Immunol 2024;154:1008-21.)

Key words: *IL-4Rα, nanobody, inhalable, asthma*

Abbreviations used

BALF:	Bronchoalveolar lavage fluid
CDR:	Complementary determining region
IC_{50}:	50% inhibitory concentration
IL-4Rα:	IL-4 receptor α chain
hIL:	Human IL
Nb:	Nanobody
OVA:	Ovalbumin
PAS:	Periodic acid-Schiff
PDB:	Protein Data Bank
SEAP:	Secreted embryonic alkaline phosphatase
STAT6:	Signal transducer and activator of transduction 6

Inhalation formulations, which provide targeted drug delivery to the airways, are consistently prioritized and recommended in the treatment of asthma due to their ability to achieve higher drug concentrations and minimize systemic side effects.[1-3] In the past decade, biologics have achieved significant success in treating asthma through various targeted mechanisms of action.[4-6] However, systemic administration of biologics in asthma treatment has limitations, including potential side effects, reduced specificity, higher dosage requirements, limited bioavailability, and patient inconvenience, emphasizing the importance of targeted delivery methods such as inhalable biologics to improve treatment efficacy and safety.[6-8]

In T2 endotype asthma, IL-4 and IL-13 play a critical role in promoting airway inflammation, bronchial hyperresponsiveness, and mucus production. These cytokines act through the IL-4 receptor signaling pathway to activate downstream pathways that drive the inflammatory processes in the airways.[9-11] Clinical evidence has confirmed the significant effectiveness of targeting the IL-4 receptor α chain (IL-4Rα) using mAbs in the treatment of T2 endotype asthma.[9-11] Considering the high expression of IL-4Rα in the airway epithelium, airway smooth muscle, and inflammatory mucosal immunocytes,[12] the development of inhalable biologics targeting IL-4Rα may offer improved efficacy and safety in treating asthma. Despite efforts to convert subcutaneously

From [a]Shanghai Novamab Biopharmaceuticals Co, Ltd, Shanghai; [b]School of Medical Technology, Shanghai University of Medicine and Health Sciences, Shanghai; [c]State Key Laboratory of Genetic Engineering, School of Life Sciences, Fudan University, Shanghai; the [d]Department of Respiratory Medicine, Shanghai Children's Medical Center, School of Medicine, Shanghai Jiao Tong University, Shanghai; [e]Shanghai Children's Medical Center Pediatric Medical Complex (Pudong), Shanghai; [f]Pediatric AI Clinical Application and Research Center, Shanghai Children's Medical Center, Shanghai; and the [g]Department of Respiratory and Critical Care Medicine of Zhongshan Hospital, Shanghai Institute of Respiratory Disease, Fudan University, Shanghai.

*These authors contributed equally to this work as co-first authors.

‡These authors contributed equally to this work as co-senior authors.

Received for publication November 20, 2023; revised May 27, 2024; accepted for publication May 31, 2024.

Available online June 11, 2024.

Corresponding author: Yakun Wan, PhD, Shanghai Novamab Biopharmaceuticals Co, Ltd, Shanghai 201318, China. E-mail: ykwan@novamab.com. Or: Yu Ding, PhD, State Key Laboratory of Genetic Engineering, School of Life Sciences, Fudan University, Shanghai 200438, China. E-mail: yuding@fudan.edu.cn. Or: Zhihong Chen, PhD, Department of Respiratory and Critical Care Medicine of Zhongshan Hospital, Shanghai Institute of Respiratory Disease, Fudan University, Shanghai 200032, China. E-mail: chen.zhihong@zs-hospital.sh.cn.

0091-6749/$36.00

https://doi.org/10.1016/j.jaci.2024.05.027

administered mAbs into inhalable biologics, the intrinsic characteristics of mAbs have posed frustrating challenges in this pursuit.[13-15]

Nanobodies (Nbs), known as single-domain antibodies, are small antibody fragments derived from camelids or engineered through recombinant techniques.[16] These unique molecules offer several advantages as inhalable biologics for asthma treatment. Their small size enables enhanced penetration into the airway epithelium, ensuring effective delivery to inflamed lung sites.[17] Nbs exhibit excellent stability, withstanding aerosolization and maintaining efficacy during storage and administration.[18] Cost-effective production using microbial systems makes them accessible for large-scale manufacturing.[19] Additionally, their high specificity allows for precise targeting of asthma-related molecules, minimizing off-target effects and enhancing safety.

In the present study, 3 IL-4Rα immunized Nb libraries were used to generate specific and functional IL-4Rα Nbs. LQ036, a bivalent Nb comprising 2 HuNb103 units, underwent evaluation for characteristics, functional activity, and crystal structure. Efficacy was assessed in ovalbumin (OVA)-induced allergic inflammation using B-hIL4/hIL4RA humanized mice. Comprehensive evaluations of pharmacokinetics, tissue biodistribution, and toxicity of LQ036 were performed. Building on the preclinical research findings, a phase IIa clinical trial of LQ036 is currently under way in China (CTR20240350), and a phase I clinical trial has been successfully completed in Australia (NCT04993443). Consequently, this work strongly suggests that LQ036 has the potential to become the first inhalable biologic treatment for asthma.

METHODS

The materials and methods regarding the *in vitro* segment are detailed in this article's Methods section in the Online Repository at www.jacionline.org.

Construction of mouse model for asthma

Female B-hIL4/hIL4RA transgenic mice (Biocytogen Pharmaceuticals Co, Ltd, Beijing, China) were intraperitoneally injected with OVA sensitizing reagent 50 μg OVA (Sigma Aldrich, St Louis, Mo) and 4 mg aluminum hydroxide gel (InvivoGen, San Diego, Calif) once weekly for a duration of 3 weeks (day 1 to day 21). The blank control group received a solvent containing aluminum adjuvant. Following the sensitization period, on day 22 to day 28, the mice in the asthma groups underwent oral and nasal atomization stimulation with OVA activator (10 mg/mL OVA) daily for 7 consecutive days. The blank control group received 0.9% sterile sodium chloride. Following sensitization and stimulation administration, the asthma model was established, with the first day of sensitization defined as day 1 of the experiment.

In vivo evaluation of drug efficacy

A total of 50 female B-hIL4/hIL4RA transgenic mice were randomly divided into 5 groups: blank control, model control, 0.2 mg/kg LQ036, 1.2 mg/kg LQ036, and 2.6 mg/kg LQ036. The asthma model was established by sensitizing the mice from day 1 to day 21 and stimulating them from day 22 to day 28. After 21 days, the mice were given LQ036 or its solvent via intratracheal administration 0.5 hours before each stimulation, once daily for 7 days. On day 28, 4 to 6 hours after the last stimulation, serum samples were collected, and OVA-specific IgE levels were measured using an ELISA kit (Biolegend, San Diego, Calif). On day 29, 24 hours after the last stimulation, bronchoalveolar lavage fluid (BALF) was collected, and CCL17, IL-4, IL-5, and IL-13 levels were quantified using Cytometric Bead Array (Biolegend). Eosinophil and neutrophil numbers were detected through peroxidase staining on a hematology analyzer (Siemens Healthcare Diagnostics, Erlangen, Germany). The mice were then dissected, and the left lung was taken for hematoxylin-eosin and periodic acid-Schiff (PAS) staining. All images were assessed by the pathologist in a blinded manner.

Mixed cellular inflammation score and mucous cell hyperplasia rate in bronchial mucosa were evaluated using the following criteria: (1) mild lesion; (2) slight lesion; (3) moderate lesion; (4) severe lesion; (5) very severe lesion. The PAS score was quantified with a 5-point grading system: 0 = <0.5% PAS-positive cells; 1 = <25% PAS-positive cells; 2 = 25% to 50% PAS-positive cells; 3 = 50% to 75% PAS-positive cells; 4 = >75% PAS-positive cells. The percentages indicate the proportion of PAS-positive cells among total airway epithelial cells. Five fields were counted for each slide, and mean PAS score was calculated from 10 mice. The procedures complied with National Research Council's Guide for the Care and Use of Laboratory Animals and were approved by the Institutional Animal Care and Use Committee at Chengdu Huaxi Haiqi Medical Technology Co., Ltd. (approval number: IACUC-A2020182-P001-01).

Mouse pharmacokinetics and biodistribution analysis

A total of 192 B-hIL4/hIL4RA double transgenic mice were randomly divided into 4 groups: 2.3 mg/kg, 5.7 mg/kg, and 11.5 mg/kg inhalation groups of LQ036 aerosol and an intravenous group receiving LQ036 aerosol (4 mg/kg), evenly distributed between males and females. The mice were given a single dose, and blood samples were collected at 5 minutes before and after dosing and 0.5, 1, 2, 4, 6, 8, 10, and 12 hours after dosing. Additionally, in the 5.7 mg/kg inhalation group and 4 mg/kg intravenous group, samples from various tissues and fluids were collected at 0.25, 4, 24, and 48 hours after dosing. In our study, the designated inhalation delivery target concentration was 4 mg/kg. Given inherent variability in aerosol concentration during each nebulization event, the meticulous calculations (delivery dose = [respiratory minute volume × nebulization time × aerosol concentration]/body weight) revealed that the delivered dose was 5.7 mg/kg. A validated ELISA method was used to determine the concentration of LQ036 in serum, tissue homogenates, and lavage fluid.

Mouse toxicity analysis

B-hIL4/hIL4RA transgenic mice were randomly assigned to 4 groups: a vehicle control group (122 mice) and 3 groups exposed to LQ036 aerosol solution at actual delivered doses of 4.3 mg/kg, 9.5 mg/kg, and 20.9 mg/kg (164 mice per group). The vehicle control group and the LQ036 groups were subjected to nasal inhalation of the vehicle control substance for 90 minutes or LQ036 aerosol solution for 20, 40, or 90 minutes once a day continuously for 4 weeks, followed by a 4-week recovery period. General conditions were observed daily, and various assessments were performed, including body weight, food consumption,

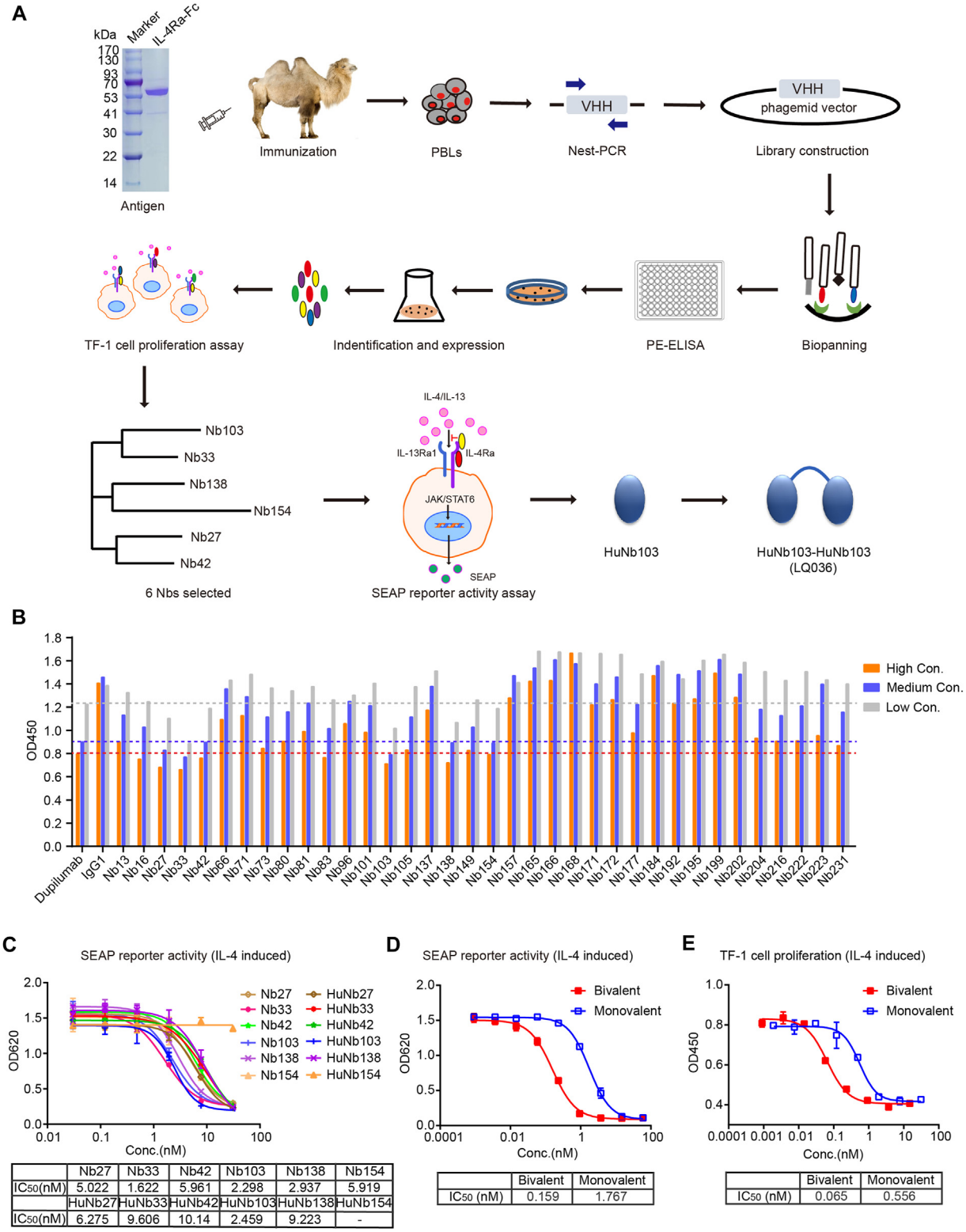

	Nb27	Nb33	Nb42	Nb103	Nb138	Nb154
IC_{50}(nM)	5.022	1.622	5.961	2.298	2.937	5.919
	HuNb27	HuNb33	HuNb42	HuNb103	HuNb138	HuNb154
IC_{50}(nM)	6.275	9.606	10.14	2.459	9.223	-

	Bivalent	Monovalent
IC_{50} (nM)	0.159	1.767

	Bivalent	Monovalent
IC_{50} (nM)	0.065	0.556

FIG 1. IL-4Rα Nbs were selected from 3 IL-4Rα immunized phage display libraries. **(A)** Screening strategy employed to isolate IL-4Rα Nbs is depicted schematically. **(B)** Cell Counting Kit 8 assay was used to determine the inhibitory effect of 38 serially diluted IL-4Rα Nbs on TF-1 cell proliferation compared with dupilumab at high, medium, and low concentrations of 1.5 μg/mL, 0.5 μg/mL, and 0.17 μg/mL. **(C)** Inhibitory effect of 6 unhumanized and humanized Nbs on SEAP reporter activity was evaluated in HEK-Blue IL-4/IL-13 cells incubated with hIL-4. **(D)** Inhibitory effect of bivalent and monovalent HuNb103 on SEAP reporter activity. **(E)** Inhibitory effects of bivalent or monovalent HuNb103 on TF-1 cell proliferation were compared. The IC_{50} value was calculated. *PE-ELISA*, Periplasmic extract ELISA, *VHH*, variable domains of the heavy-chain antibodies.

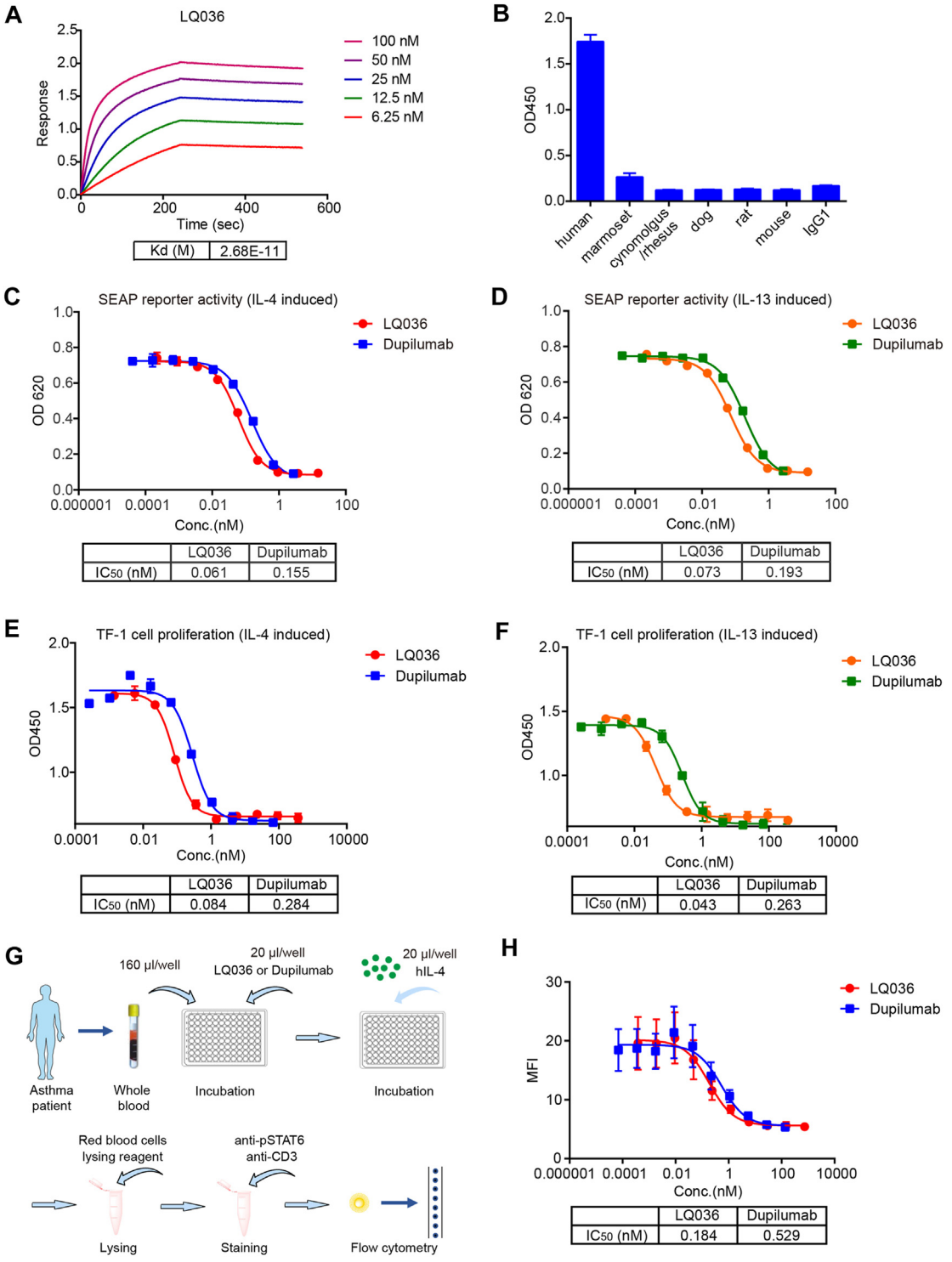

FIG 2. Characterization and functional activity of LQ036. **(A)** Affinity of LQ036 to IL-4Rα was assessed using Fortebio detection. **(B)** Specificity of LQ036 toward human IL-4Rα compared with marmoset, cynomolgus/rhesus, dog, rat, and mouse antigens was determined using ELISA. **(C** and **D)** Inhibitory effects of LQ036 and dupilumab on SEAP reporter activity were evaluated in HEK-Blue IL-4/IL-13 cells incubated with hIL-4 *(C)* or hIL-13 *(D)*. **(E** and **F)** Inhibitory effects of LQ036 and dupilumab on TF-1 cell proliferation induced by hIL-4 *(E)* or hIL-13 *(F)* were determined. IC_{50} values were calculated. The above experiments were performed in triplicate, and data were presented as mean ± SD. **(G)** Experimental design depicting the effect of LQ036 on phosphorylated STAT6 (pSTAT6) in T cells from patients with asthma. **(H)** Statistic of the inhibitory effect of LQ036 and dupilumab on pSTAT6 in T cells from 7 patients with asthma. IC_{50} value was calculated. The data represent mean ± SEM. *MFI,* Mean fluorescence intensity; *OD,* optical density.

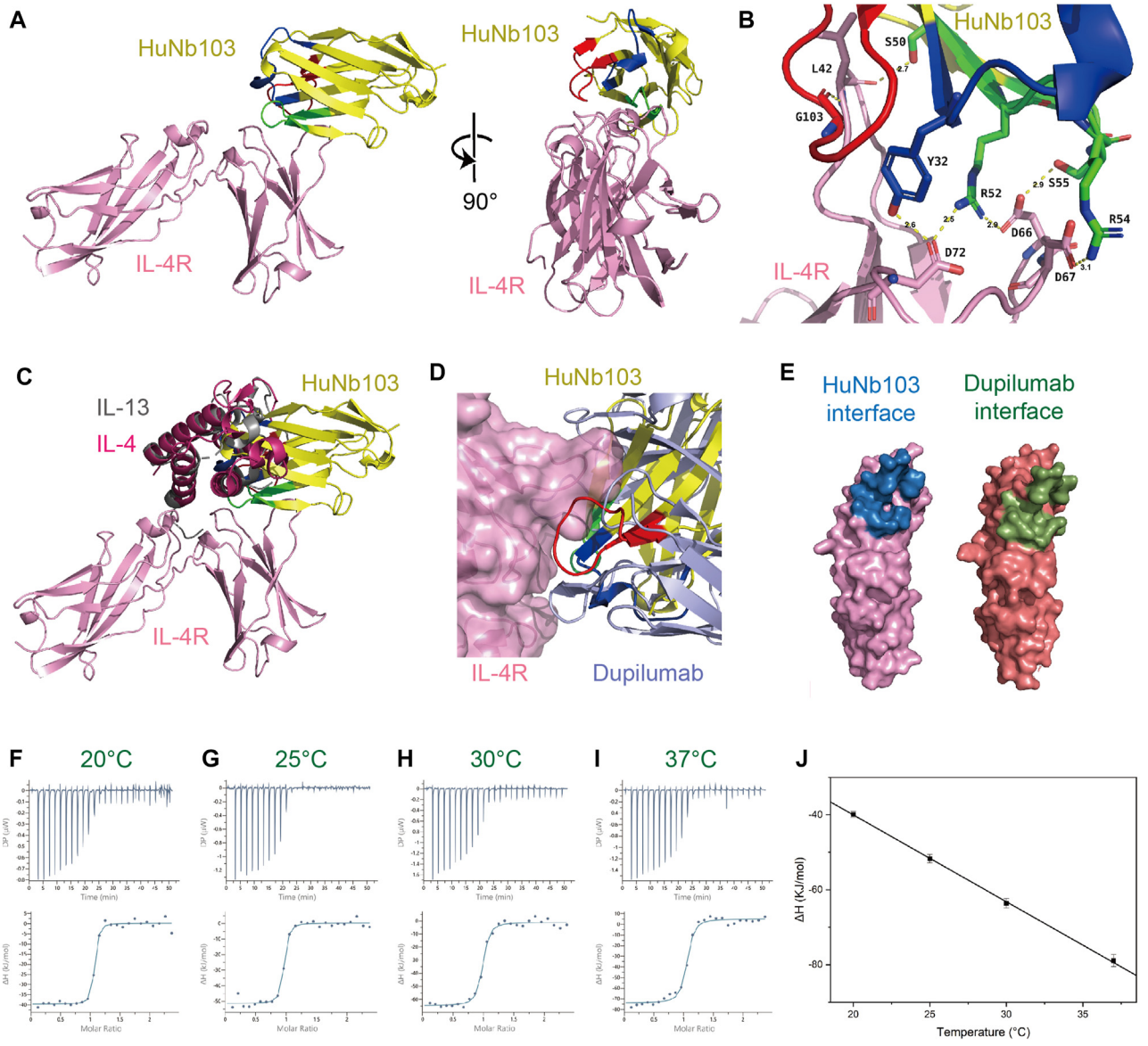

FIG 3. Crystal structure and interactions of the HuNb103:IL-4Rα complex. **(A)** Schematic representation of the HuNb103:IL-4Rα heterodimer, highlighting the overall structure of the complex. **(B)** Detailed interactions between HuNb103 CDRs and IL-4Rα, highlighting key residues involved. **(C)** Aligning HuNb103 structures with IL-4 (PDB: 3BPN) and IL-13 (PDB: 3BPO) when competing for binding to IL-4Rα highlights the shared binding site. **(D)** Aligning HuNb103 structures with dupilumab (PDB: 6WGL) when bound to IL-4Rα highlights structural differences. **(E)** Comparison of the binding interfaces of IL-4Rα with HuNb103 and dupilumab. In the figures, HuNb103 is depicted in *yellow*; CDR1, *blue*; CDR2, *green*; and CDR3, *red*. IL-4Rα is shown in *pink*. Hydrogen bonds are represented by *yellow dashed lines* and salt bridges by *blue dashed lines*; key residues are depicted as *sticks*. **(F-I)** Original isothermal titration calorimetry data for HuNb103:IL-4Rα at 20°C, 25°C, 30°C, and 37°C. Each subfigure shows raw data (*upper*) and a fitted curve (*lower*). The y-axis represents differential power between the sample and reference cells. The x-axis of the *lower panels* represents the molar ratio, and the y-axis represents the molar change of calories in the syringe. *Dots* represent the acquired data in experiments, and *lines* represent the fitted curve. **(J)** ΔH as a function of temperature for HuNb103:IL-4Rα. The slope of a regression line was used to define the ΔCp of the interaction. *DP,* Differential power.

ophthalmologic examination, functional observational battery test, respiratory measurements, cytokines, T lymphocytes, and subset measurements.

After the last dose and the recovery period, 58 and 38 mice per group, respectively, were euthanized for organ weight measurement, hematologic analysis, blood biochemistry, immunoglobulin, complement, circulating immune complex, and serum anti-drug antibody testing. Meanwhile, after the last dose and the recovery period, 20 and 10 mice per group, respectively, underwent gross anatomic observation, bone marrow smears, organ weight measurement, and histopathologic examination.

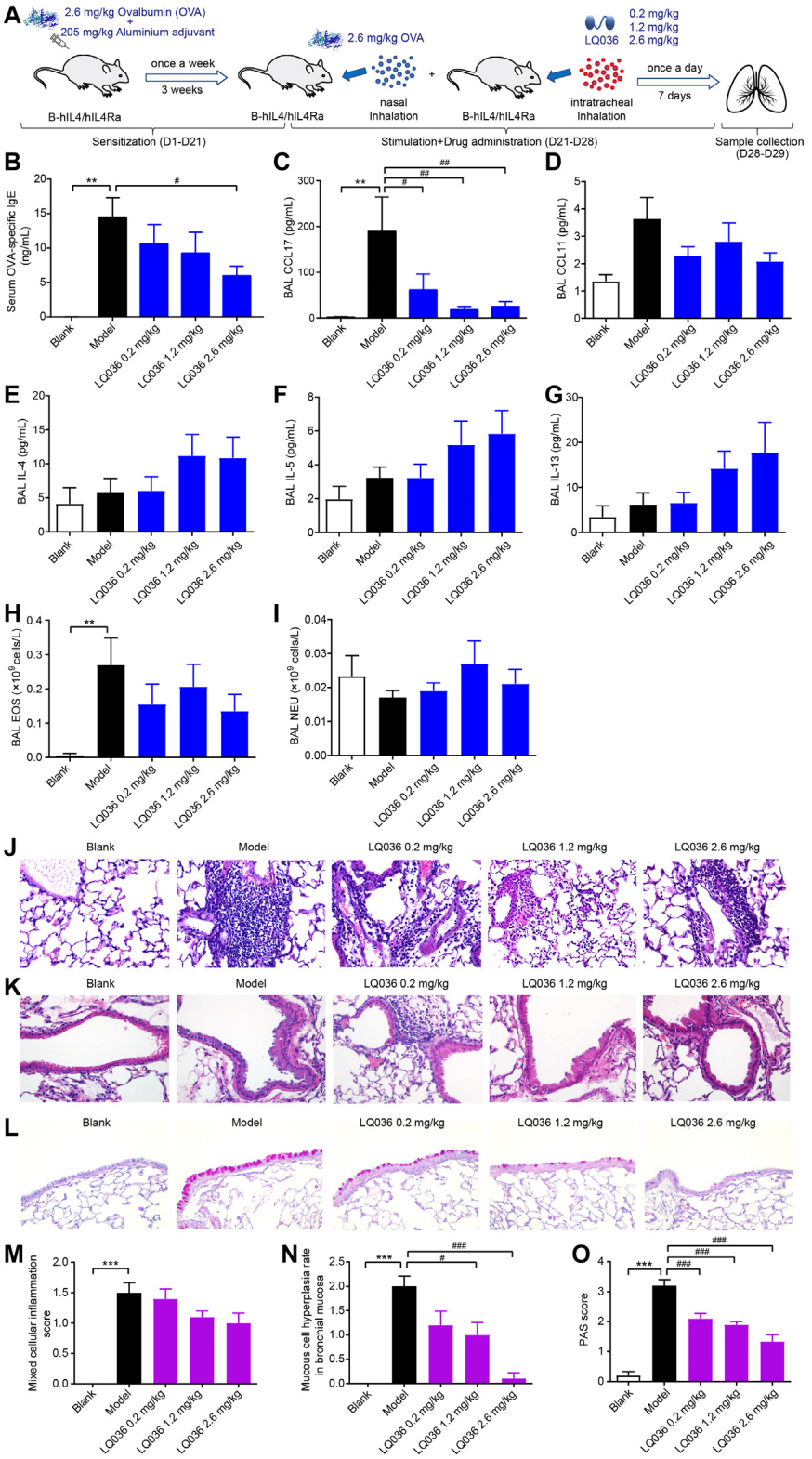

FIG 4. Drug efficacy of LQ036 on OVA-induced acute allergic inflammation in B-hIL4/hIL4RA humanized transgenic mice. **(A)** Schedule of the allergic inflammation mouse model establishment and intratracheal inhalation of LQ036. **(B)** Measurement of serum OVA-specific IgE levels on day 28 (4-6 hours after the last stimulation) using an ELISA kit. **(C** and **D)** Quantifying chemokines including CCL17 *(C)* and CCL11 *(D)* levels in BALF on day 29 using a cytometric bead array. **(E-G)** Assessment of cytokine levels including IL-4 *(E)*, IL-5 *(F)*, and IL-13 *(G)* in BALF on day 29 using a cytometric bead array. **(H** and **I)** Measurement of eosinophil *(H)* and neutrophil *(I)* numbers in BALF on day 29 through peroxidase staining. **(J** and **K)** Effect of LQ036 on mixed cellular inflammation *(J)* and bronchial mucous cell hyperplasia *(K)* of the lung assessed through

Statistical analysis

Data are expressed as the mean ± SD or mean ± SEM. A *t* test (for data with homogeneity of variance) or Mann-Whitney *U* test (for data with nonhomogeneity of variance) was used to compare the blank control and model groups. For the pairwise comparisons between the model control group and the treatment groups, the least significant difference test (for data with homogeneity of variance) or Mann-Whitney *U* test (for data with nonhomogeneity of variance) was used. All tests were two-tailed. Statistical analysis was performed using Stata/IC 15.0.

RESULTS

Anti-IL-4Rα–specific Nbs screened from phage display library

To construct an anti-IL-4Rα Nb phage display library, 3 camels were immunized with IL-4Rα fused to Fc (IL-4Rα–Fc) with high purity (Fig 1, *A*). After 7 immunizations, PBLs were collected to create the phage display library. The 3 libraries had capacities totaling 1.5×10^9, 1.1×10^9, and 1.0×10^9 colony-forming units, respectively, with insert ratios ranging from 91.6% to 95.8%, indicating excellent quality and diversity across the libraries. Following 3 rounds of phage display biopanning, the fold enrichment of IL-4Rα–specific variable domains of the heavy-chain antibodies derived from 3 libraries reached 1166, 1685, and 2419 times, respectively (Table E1 in the Online Repository at www.jacionline.org).

Through periplasmic extract ELISA and sequencing analysis, 38 specific anti-IL-4Rα Nbs were screened, which belong to different families with the variations in complementary determining region 3 (CDR3) higher than 70% (data not shown). Subsequently, 6 Nbs (Nb27, Nb33, Nb42, Nb103, Nb138, and Nb154) were selected based on TF-1 cell proliferation, which displays higher inhibitory effect compared with the positive control dupilumab, at 3 diluted concentrations of 1.5 μg/mL, 0.5 μg/mL, and 0.17 μg/mL (Fig 1, *B*). These 6 Nbs were then humanized to minimize immunogenicity. Thereafter, the inhibitory effect of these 6 pre- or post-humanized Nbs on secreted embryonic alkaline phosphatase (SEAP) reporter activity were determined in HEK-Blue IL-4/IL-13 cells (Invivogen, San Diego, Calif) incubated with human IL-4 (hIL-4), and their 50% inhibitory concentration (IC_{50}) were displayed. As illustrated in Fig 1, *C*, huNb103 exhibited the most potent inhibitory effect on SEAP reporter activity after humanization. To enhance the functional efficacy of huNb103, we developed a bivalent construct named LQ036, consisting of 2 huNb103 units linked together. LQ036 displayed a higher inhibitory effect on SEAP reporter activity and TF-1 cell proliferation compared with the monovalent huNb103, with IC_{50} values of 0.159 nM vs 1.767 nM and 0.065 nM vs 0.556 nM, respectively (Fig 1, *D* and *E*).

High affinity, specificity, and functional activity of LQ036

To characterize LQ036, we assessed its affinity and binding specificity. It exhibited high affinity (equilibrium dissociation constant = 2.68×10^{-11} M) and was specifically bound to human IL-4Rα, not to other species (marmoset, cynomolgus/rhesus, dog, rat, and mouse) (Fig 2, *A* and *B*). Additionally, this binding exhibited high specificity for IL-4Rα, with no binding detected to structurally related cytokine receptors such as IL-6Rα, IL-17Rα, IL-18Rα, or IL-23Rα (Fig E1 in the Online Repository at www.jacionline.org).

In vitro studies revealed that LQ036 exhibited higher inhibitory effects on SEAP reporter activity in HEK-Blue IL-4/IL-13 cells when incubated with hIL-4 or hIL-13 compared to dupilumab (IC_{50}: 0.061 nM vs 0.155 nM or 0.073 nM vs 0.193 nM) (Fig 2, *C* and *D*). Similarly, LQ036 demonstrated superior inhibitory effects on TF-1 cell proliferation when incubated with hIL-4 or hIL-13 compared with dupilumab (IC_{50}: 0.084 nM vs 0.284 nM or 0.043 nM vs 0.263 nM) (Fig 2, *E* and *F*). Furthermore, compared with dupilumab, LQ036 demonstrated a more potent inhibitory effect on signal transducer and activator of transduction 6 (STAT6) phosphorylation in T cells from patients with asthma (IC_{50}: 0.184 nM vs 0.529 nM) (Fig 2, *G* and *H*). The inhibitory effects of LQ036 on phosphorylated STAT6 in T cells obtained from 7 individual patients with asthma and the primary data from fluorescence-activated cell sorting plots are displayed in Fig E2 (in the Online Repository at www.jacionline.org). Combining *in vitro* and *in vivo* results, LQ036 exhibited better functional activity than dupilumab.

Analysis of HuNb103:IL-4Rα complex structure

We obtained the HuNb103:IL-4Rα complex through size-exclusion chromatography and determined its x-ray structure, providing atomic-level insights into the interaction (Fig E3 and Table E2 in the Online Repository at www.jacionline.org). The crystal belonged to space group P 1 21 1, with each asymmetric unit comprising 2 IL-4Rα extracellular domain antigen chains and 2 HuNb103 Nb chains (Fig 3, *A*). The glycosylation of the aspartic acid side chain of IL-4Rα was observed near multiple asparagine residues. The extracellular region of the antigen had the cytokine receptor homology and immunoglobulin-like domains, with HuNb103 mainly interacting with the first cytokine receptor homology domain. The detailed analysis revealed interactions involving all CDRs of HuNb103 (Fig 3, *B*). Notably, CDR2 played a crucial role, forming multiple hydrogen bonds and salt bridges with Leu42, Asp66, Asp67, and Asp72 of IL-4Rα, through key residues of Ser50, Arg52, Arg54, and Ser55. The extensive interactions between positively charged residues in the arginine cluster of HuNb103 and negatively charged residues in the aspartic acid cluster of IL-4Rα were significant. Additionally, strong hydrogen bonds were observed between Tyr32 of CDR1 and Asp72 of IL-4Rα and between Gly103 of CDR3 and Leu42 of IL-4Rα (Fig 3, *B*). The structural information of the complex is deposited in the Protein Data Bank (PDB) (ID: 8K4Q), and the Crystal structure of HuNb103 bound to IL-4Rα available at https://www.rcsb.org/structure/8K4Q.

We present the alignment of HuNb103 structures with IL-4 and IL-13, competing for binding to IL-4Rα. This alignment highlights their similarities in binding modes, targeting the same IL-

hematoxylin-eosin staining. Representative hematoxylin-eosin–stained sections are displayed. **(L)** Effect of LQ036 on airway goblet cell hyperplasia and mucus secretion assessed via PAS staining. Representative PAS-stained sections are displayed. Images were obtained at 400×. **(M-O)** Evaluation of mixed cellular inflammation scores *(M)*, bronchial mucous cell hyperplasia rates *(N)*, and PAS scores *(O)* of the lung. n = 9-10 mice per group. Blank group indicates healthy/nonimmunized/nontreated mice. Data are presented as mean ± SEM. ***P* < .01; ****P* < .001 versus Blank; #*P* < .05; ##*P* < .01; ###*P* < .001 versus Model. *BAL,* Bronchoalveolar lavage; *EOS,* eosinophils; *NEU,* neutrophils.

4Rα site (Fig 3, *C*). Comparing the binding sites of HuNb103 and dupilumab with IL-4Rα, the overall binding regions are similar, explaining their comparable mechanisms of action (Fig 3, *D* and *E*). HuNb103:IL-4Rα binding affinity was measured using isothermal titration calorimetry across a temperature spectrum of 20°C to 37°C, showing a strong and stable 1:1 bimolecular association with equilibrium dissociation constant values ranging from 7.47 to 27.8 nM and a highly negative overall free energy change (ΔG about −45 kJ/mol) (Fig 3, *F-J*; Table E3 in the Online Repository at www.jacionline.org). Furthermore, HuNb103 demonstrated a higher affinity for IL-4Rα compared with dupilumab, as indicated by the calculated free energy of binding (ΔiG) of −6.5 kcal/mol versus −2.8 kcal/mol, determined through polymerization-induced self-assembly analysis (Table E4 in the Online Repository at www.jacionline.org).

Suppression of OVA-induced acute allergic inflammation in humanized mice with intratracheal inhalation of LQ036

To evaluate the therapeutic impact of LQ036 on allergic inflammation, we employed B-hIL4/hIL4RA humanized mice. These mice were sensitized and stimulated with OVA for 21 days, followed by daily intratracheal inhalation of LQ036 or its solvent for 7 consecutive days. The entire experimental protocol is presented in Fig 4, *A*.

The results demonstrated that LQ036 administration led to a reduction in OVA-specific IgE levels in serum on day 28 in a dose-dependent manner (Fig 4, *B*). Furthermore, all 3 doses of LQ036 significantly decreased CCL17 levels in BALF on day 29 (Fig 4, *C*), while also reducing CCL11 production, albeit without reaching statistical significance (Fig 4, *D*). Notably, LQ036 did not inhibit the expression of key T_H2 cytokines in BALF, including IL-4, IL-5, and IL-13, but rather stimulated their expression to some extent (Fig 4, *E-G*). Given the pivotal role of eosinophils in the development of allergic inflammation, we assessed the impact of LQ036 on eosinophil production in BALF (Fig 4, *H*). The result indicated that LQ036 inhibited eosinophil production in the OVA-induced allergic inflammation model, although the decrease was not statistically significant. Additionally, LQ036 exhibited no discernible impact on neutrophils (Fig 4, *I*).

The histopathologic analysis further revealed that LQ036 suppressed mixed cellular inflammation in lung and bronchial mucous cell hyperplasia in a dose-dependent manner, as indicated by the mixed cellular inflammation score (Fig 4, *J* and *M*) and bronchial mucous cell hyperplasia rates (Fig 4, *K* and *N*). Detailed information regarding the suppressive effects is presented in Table E5 (in the Online Repository at www.jacionline.org). Concurrently, PAS staining demonstrated that LQ036 exhibited a dose-dependent decrease in goblet cell hyperplasia and mucus secretion in the airways (Fig 4, *L* and *O*). The specific impact of LQ036 on PAS scores is shown in Table E6 (in the Online Repository at www.jacionline.org). Consequently, these findings strongly indicate that inhalation administration of LQ036 has significant potential for alleviating allergic inflammation.

Nasal inhalation pharmacokinetics and toxicity of LQ036 in B-hIL4/hIL4RA humanized mice

B-hIL4/hIL4RA humanized mice were used to evaluate the pharmacokinetics and tissue biodistribution of LQ036 following nasal inhalation or intravenous injection (Fig 5, *A*). The amount of LQ036 deposited in the lungs, including left lung, right lung (lavaged), and lung lavage fluid, increased proportionally with the dose at 0.25 hour after atomization. Meanwhile, inhalation resulted in significantly higher lung LQ036 levels compared with intravenous injection (Fig 5, *B*). For instance, the maximum observed serum concentration and area under the curve up to the last quantifiable time point of LQ036 in the lungs after 5.7 mg/kg intranasal exposure at 0.25 hour were 54 times and 234 times higher, respectively, than that after 4 mg/kg treatment in the intravenous injection group (Table I).

Subsequently, we assessed the pharmacokinetics and biodistribution of LQ036 following 5.7 mg/kg inhalation or 4 mg/kg intravenous injection. As illustrated in Fig 5, *C*, the pharmacologic concentration of LQ036 with 5.7 mg/kg inhalation exhibited a consistent pattern in left lung, right lung (lavaged), and lung lavage fluid, with a terminal phase half-life of approximately 6 hours (Table I). Notably, LQ036 maintained relatively high concentration levels within 4 hours after administration and remained detectable even after 48 hours, whereas it became undetectable in the 4 mg/kg intravenous injection group after 24 hours (Fig 5, *C* and *D*).

In the 5.7 mg/kg inhalation group, LQ036 was primarily distributed within the lower respiratory system (lungs, buccal mucosa, and main bronchi), followed by distribution in the serum, brain, kidneys, and heart (Fig 5, *C*). For example, the maximum observed serum concentration and area under the curve up to the last quantifiable time point of LQ036 in left lung were 1034 times and 694 times higher compared with these values in serum (Table I). Conversely, in the 4 mg/kg intravenous injection group, LQ036 showed a predominant distribution in the kidneys and serum, followed by the buccal mucosa, lungs, and main bronchi. Notably, owing to the molecular weight of LQ036 being less than 60 kDa, the kidneys emerged as the principal organ responsible for the elimination of LQ036 in this context (Fig 5, *D*). Consequently, inhalation administration of LQ036 led to its main distribution within the respiratory system, underscoring the advantageous delivery potential of inhalation administration.

The toxicity detection of LQ036 revealed that the no-observed-adverse-effect level was 20.9 mg/kg. The exposure amounts of LQ036 atomizing solution after the last administration at this dose were 49,900 h·ng/mL and 16,700 h·ng/mL, respectively. Table II shows that no obviously toxicologic changes were observed across various parameters. Specifically, the cytokine indicators, including IL-2, IL-6, IL-10, IFN-γ, and TNF-α, and immune-related indicators, such as IgA, IgG, C3, CIC, T lymphocytes, $CD4^+$ and $CD8^+$ T lymphocytes, and $CD4^+/CD8^+$ ratio (excluding IgM), showed no significant abnormalities. It is noteworthy that during the period from the end of administration to the end of recovery period, anti-drug antibodies were detected only in individual mice within certain groups receiving LQ036 atomizing solution. This suggests that the LQ036 atomized solution demonstrated a low level of immunogenicity in B-hIL4/hIL4RA mice (Table II).

Developability of LQ036

We further evaluated the developability of LQ036 based on its functional studies in both *in vivo* and *in vitro* settings. Large-scale production of LQ036 was carried out in a yeast system, yielding

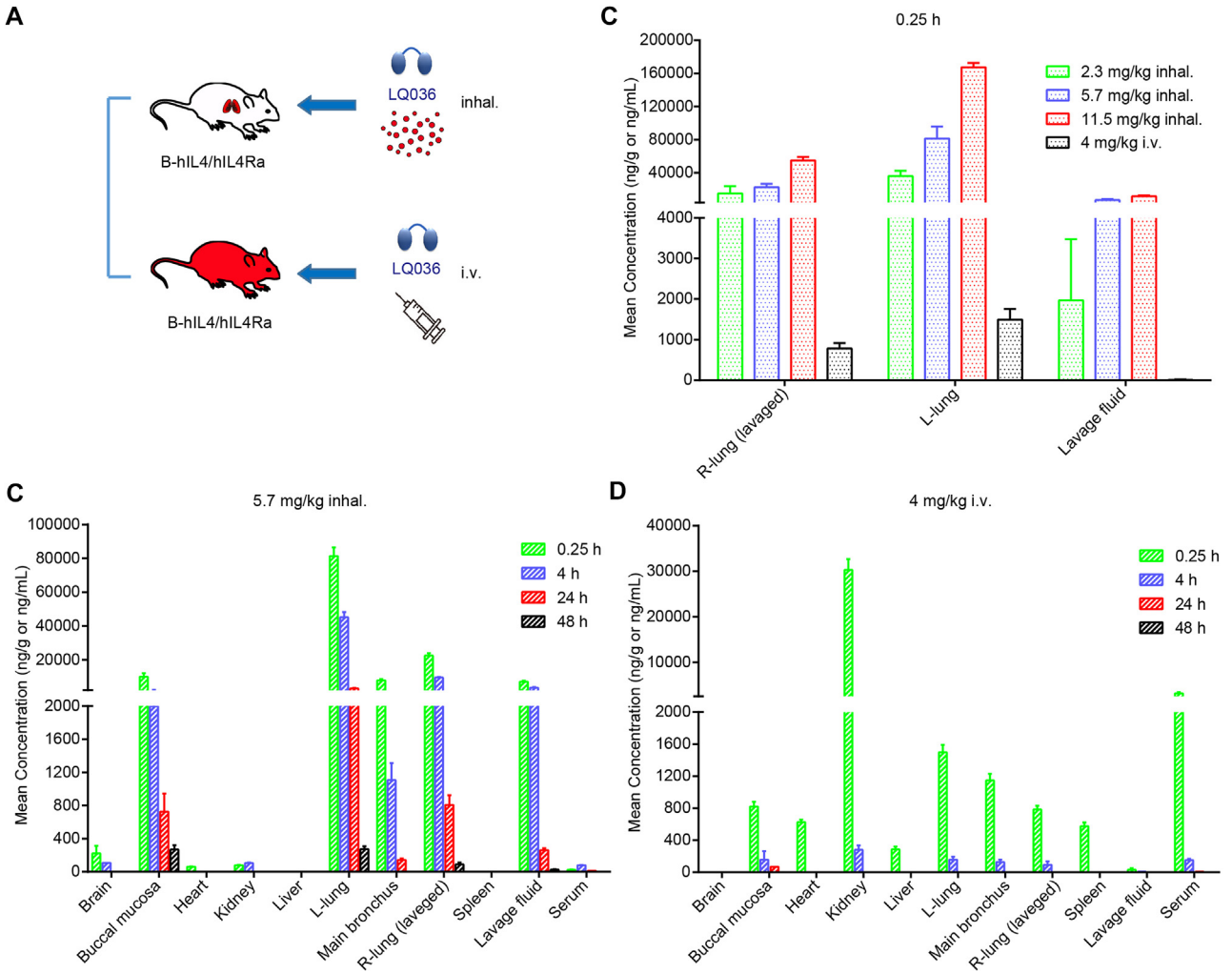

FIG 5. Pharmacokinetics and tissue biodistribution of LQ036 in B-hIL4/hIL4RA humanized mice. **(A)** Schematic representation of drug delivery method. **(B)** LQ036 concentration was measured in right lung (lavaged), left lung, and lavage fluid at 0.25 hour after nasal inhalation of 2.3 mg/kg, 5.7 mg/kg, 11.5 mg/kg or intravenous injection of 4 mg/kg. **(C** and **D)** Biodistribution of LQ036 in B-hIL4/hIL4RA mice after inhalation of 5.7 mg/kg *(C)* or intravenous administration of 4 mg/kg *(D)* within 48 hours. Data are presented as mean ± SEM. inhal., inhalation; i.v., intravenous injection; L-lung, left lung; R-lung, right lung.

4.2 g/L of LQ036 after 140 hours in a 100-L fermenter (Fig 6, *A*). Subsequently, following affinity chromatography, hydrophobic chromatography, and molecular sieve chromatography purification procedures, LQ036 exhibited high purity, as demonstrated by reductive SDS-PAGE analysis (Fig 6, *B*). Furthermore, most of the nebulized LQ036 particles were distributed within the range of 0.98 to 14.1 μm, suggesting efficient delivery to the lungs (Fig 6, *C*). Pre-nebulized and post-nebulized LQ036 showed purity of 98.5% and 97.6%, respectively, according to size-exclusion HPLC analysis (Fig 6, *D*).

Functional evaluations of post-nebulized LQ036 *in vitro* demonstrated similar inhibitory effects as pre-nebulized LQ036 on SEAP reporter activity in HEK-Blue IL-4/IL-13 cells (Fig 6, *E*). Long-term stability analysis confirmed that LQ036 remained stable after 24 months at −20°C, with greater than 96.5% in the monomeric form (Fig 6, *F*). In summary, we successfully obtained LQ036 with high yield, purity, satisfactory nebulization characteristics, and good stability in a yeast expression system.

DISCUSSION

Here we describe the discovery and characteristics of LQ036, a bivalent Nb targeting IL-4Rα with high specificity and affinity. Its small molecular weight facilitates facile absorption by epithelial cells and excellent tissue permeability. Additionally, stable physicochemical properties make it highly tolerant to physical stress in respiratory formulations. In humanized mouse models, inhalation of LQ036 achieves maximum lung exposure, effectively inhibiting inflammation and mucous cell hyperplasia induced by OVA. Furthermore, LQ036 can be produced on a large scale at a low cost in yeast cells, greatly reducing the economic burden of once-daily dosing of the inhaled biopharmaceutical. These findings support the potential use of LQ036 as an inhalation therapy for asthma.

Biological activity is one of the most important considerations in drug development, as higher biological activity usually signifies better therapeutic potential. Regarding biological functionality, LQ036 exhibits significantly higher inhibitory capability against IL-13/IL-4–induced cell

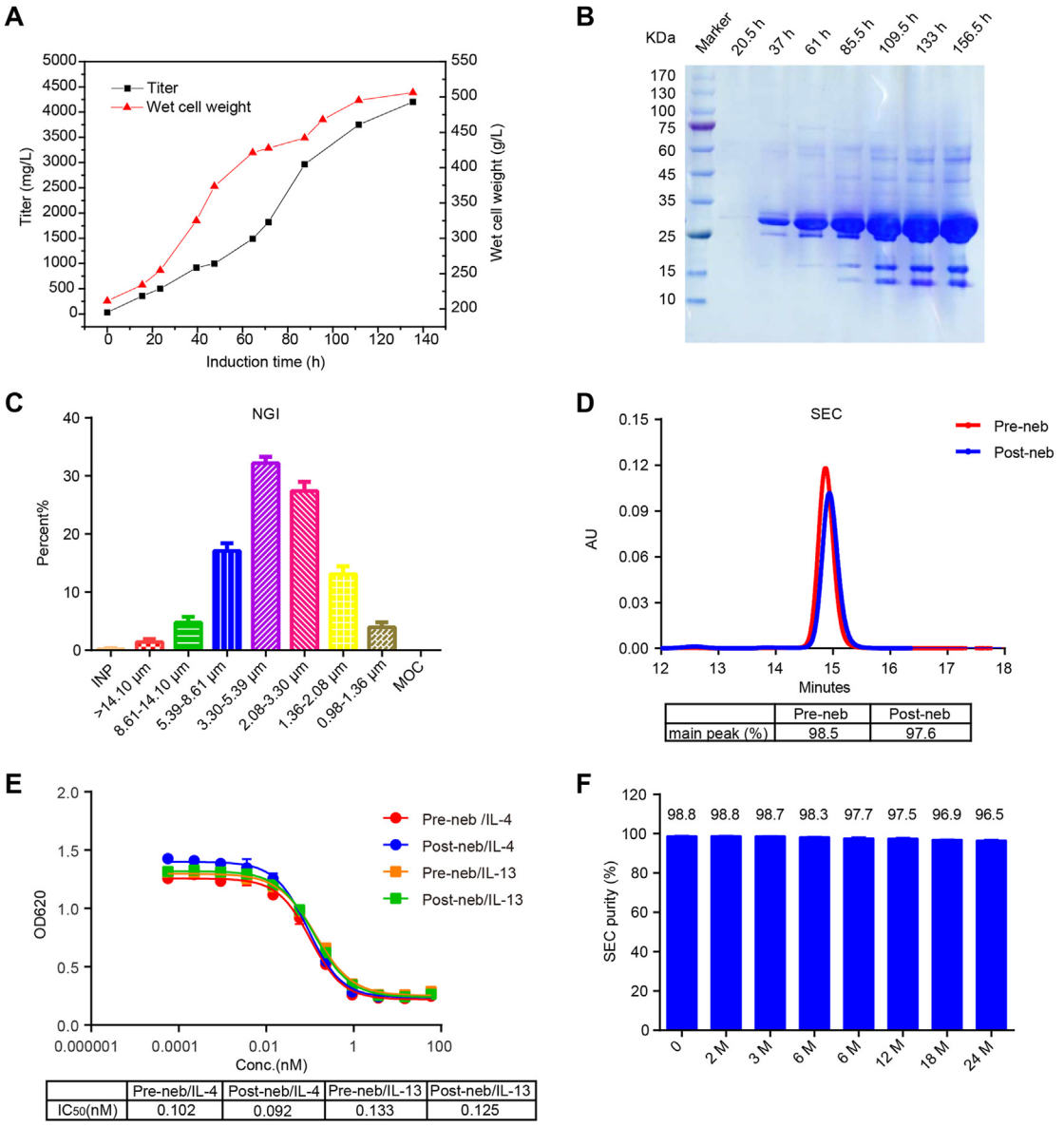

FIG 6. Large-scale production of LQ036 and its developability analysis. **(A)** Protein titer and wet cell weight of LQ036 in the fermentation tank were measured at the indicated times. **(B)** Protein expression of LQ036 was detected through SDS-PAGE. **(C)** Size distribution was detected by the Next-Generation Pharmaceutical Impactor. **(D)** Purity of LQ036 pre- or post-nebulization was determined through size-exclusion HPLC analysis. **(E)** Inhibitory effect of LQ036 pre- or post-nebulization toward the SEAP reporter activity in HEK-Blue IL-4/IL-13 cells incubated with hIL-4 or hIL-13. **(F)** Long-term stability of LQ036 was determined through size-exclusion HPLC analysis. Data were presented as mean ± SD. *AU,* Absorbance unit; *INP,* induction port; *MOC,* microporous collector; *NGI,* Next-generation pharmaceutical impactor; *Post-neb,* post-nebulization; *Pre-neb,* pre-nebulization; *SEC,* size-exclusion chromatography.

proliferation and IL-4–induced phosphorylation of STAT6 compared with dupilumab. One possible explanation is that LQ036 binds to IL-4Rα with higher affinity compared with dupilumab. After polymerization-induced self-assembly analysis, despite the similar interface area upon binding, the calculated free energy of binding (ΔiG) was −6.5 kcal/mol for HuNb103 and −2.8 kcal/mol for dupilumab, indicating a higher affinity for IL-4Rα, which resulted in more stable and more robust interactions. The dimerized form of HuNb103, known as LQ036, further enhances its affinity for IL-4Rα, suggesting superior therapeutic potential. Another contributing factor is the improved tissue penetration ability of Nbs. Due to their small size and compact structure, Nbs have better access to target tissues and can penetrate deeper into tissues than larger antibodies such as dupilumab, potentially leading to better targeting and engagement with IL-4Rα in various tissues, enhancing its therapeutic effects.

Inhalation delivery offers advantages for pulmonary diseases due to rapid absorption and localized action in the lungs, reducing systemic exposure and increasing safety.[14,20] For inhalable biopharmaceuticals, favorable physicochemical properties are essential to withstand the stresses encountered during production,

TABLE I. Pharmacokinetics parameters of LQ036 after 5.7 mg/kg inhalation or 4 mg/kg intravenous administration

Group	Tissue	$T_{1/2}$ (h)	T_{max} (h)	C_{max} (ng/mL or ng/g)	AUC_{0-t} (h·ng/mL or h·ng/g)	MRT_{0-t} (h)
5.7 mg/kg inhalation	Lung	6.0	0.25	81,500	770,000	5.1
	Lung (lavage)	6.6	0.25	22,500	177,000	5.3
	Lavage fluid	6.3	0.25	7,070	62,400	5.2
	Serum	—	4	78.8	1,110	6.1
4 mg/kg intravenous injection	Lung	—	0.25	1,500	3,290	0.59
	Lung (lavage)	—	0.25	782	1,740	0.62
	Lavage fluid	—	0.25	11.2	32.0	1.4
	Serum	—	0.25	3,150	8,610	1.1

AUC_{0-t}, Area under the curve up to the last quantifiable time point; C_{max}, maximum observed serum concentration; MRT_{0-t}, mean residence time; $T_{1/2}$, half-life; T_{max}, time to maximum serum concentration.

TABLE II. Toxicology of LQ036

Parameters	Major findings at end of dosing or before	Major findings at end of recovery period)
Mortality	None	None
Clinical signs	None	None
Body weight	All body weight changes <4.62%, which means no toxicologic significance	None
Ophthalmoscopy	None	None
Urinalysis	None	None
Food consumption	None	None
FOB	None	None
Respiratory function	None	None
Hematology	Transient RBC, HGB, HCT increase (<7.16%), with no toxicology significance	None
Blood biochemistry	All transient ALB, CK, ALP and A/G increase changes <30%, concluded as no toxicologically meaningful significance	None
Cytokines	None	None
Immune-related indicators	None (excluding IgM)	None (excluding IgM)
Gross anatomic observations	None	None
Organ weights and coefficients	None	None
Histopathology	None	None
Anti-LQ036 antibody	Proportions of anti-LQ036 antibodies detected in 4.3, 9.5, and 20.9 mg/kg/d groups were 0/8, 2/8, and 1/8	Proportions of anti-LQ036 antibodies detected in 4.3, 9.5, and 20.9 mg/kg/d groups were 1/8, 0/7, and 1/8

A Good Laboratory Practice–compliant repeat dose toxicology study was performed with doses 4.3, 9.5, and 20.9 mg/kg.
A/G, Albumin/globulin; *ALB,* albumin; *ALP,* alkaline phosphatase; *CK,* creatine kinase; *FOB,* functional observational battery; *HCT,* hematocrit; *HGB,* hemoglobulin; *RBC,* red blood cell (count).

nebulization, and transportation. However, traditional large biologics face challenges in developing inhalable formulations due to their large size and structural instability.[13,15] Nbs, with their robustness and physicochemical stability, can be delivered via nebulization without losing potency.[17] Our inhalable Nb against the coronavirus SARS-CoV-2 demonstrated high viral neutralization properties in preclinical studies.[21] Additionally, other inhalable Nbs, such as ALX-0171 targeting respiratory syncytial virus, have entered clinical development.[22,23] Our data demonstrate the high stability of LQ036 during nebulization and strong biological activity in preclinical studies. These findings provide solid support for its advancement into clinical development, with the noteworthy achievement that a phase IIa clinical trial of LQ036 has already commenced in China, and a phase I clinical trial has been completed in Australia.

It is worth noting that we observed an increase in T_H2-dependent cytokines, including IL-4, IL-13, and IL-5, in BALF following LQ036 administration, although there were no statistical differences. Consistent with this, previous studies have reported heightened levels of IL-4, IL-13, or IL-5 in patients treated with dupilumab, which targets IL-4Rα.[24,25] While the precise reasons for the increase in T_H2 cytokines remain unclear, we speculate that the inhibition of IL-4Rα may induce a compensatory phenomenon in T_H2 T cells and innate lymphoid cells, which are the primary sources of these cytokines. Considering that IL-4, IL-13, and IL-5 are pivotal factors driving type 2 inflammation in asthma, theoretically, the inhibition of IL-4Rα may yield unfavorable effects. However, given that IL-4 and IL-13 directly exert their influence on different cells through IL-4Rα, contributing to inflammation and airway remodeling,[26] the use of LQ036 or dupilumab to selectively block the functionality of IL-4Rα effectively mitigates the adverse consequences associated with the increase in IL-4 and IL-13. On the contrary, it is essential to consider the impact of IL-4Rα blockade on IL-5 increase in asthma. The primary role of IL-5 is to promote the maturation, survival, proliferation, and activation of eosinophils.[27] Although LQ036 leads to an

increase in IL-5, the substantial reduction in eosinophils in the lung compared with the model group may be attributed to LQ036 blocking the IL-4/IL-13–IL-4R signaling pathway, a crucial regulatory factor for eosinophils entering peripheral tissues.[28,29] The mechanism of inflammatory cell mobilization in allergic asthma is intricate and involves various cell types. Due to the limitations of the model and the detection indicators employed in this study, further comprehensive research and clinical investigation are warranted to elucidate the impact of targeting IL-4Rα inhibition. However, the observed phenomenon in this study provides insights into the divergent clinical practices of biological agents targeting IL-4Rα and IL-5R (or inhibiting IL-5) in the treatment of type 2 inflammation in asthma.

The rapid onset of action is crucial in asthma treatment, making inhaled formulations preferable. IL-4Rα is primarily expressed in airway epithelium, airway smooth muscle, inflammatory mucosal immunocytes, and endothelial cells, providing crucial support for the swift therapeutic effects achievable with inhaled biologics targeting IL-4Rα.[12,30] Preclinical data for LQ036 show that after nebulized inhalation at 5.7 mg/kg, peak lung concentration reaches 81,500 ng/mL within 0.25 hour. This concentration is more than 100 times higher than the IC_{90} values associated with SEAP reporter activity and TF-1 cell proliferation, indicating significant efficacy in inhibiting IL-4/IL-13–mediated signaling. These data support the potential for rapid onset of action with LQ036 in asthma treatment. In comparison, dupilumab, a systemic therapy targeting IL-4Rα for atopic asthma, shows clinically significant improvement in patients after 2 weeks of treatment.[31] Additionally, the half-life of 5.7 mg/kg LQ036 in humanized mouse lungs is up to 6 hours. These results support the clinical design of once-daily dosing for LQ036. PRS060, an inhaled biologic targeting IL-4Rα, was administered twice daily in phase 2 clinical trials (NCT04643158).[30,32]

Our toxicity assessment of LQ036 in preclinical studies revealed no discernible toxicologic alterations. Notably, compared with intravenous administration, inhalation administration allows a minimal amount of the drug to traverse olfactory bulb and reach the brain.[33] In response to this phenomenon, focused observations were conducted in nonclinical toxicology experiments. Our findings indicate that no damage was observed in brain tissue, and no abnormalities were detected in the mouse functional observational battery experiment. Furthermore, our ongoing clinical single ascending dose and multiple ascending dose studies have not revealed any discernible impact on the memory or cognition of the study subjects (data not shown). Consequently, we will continue to monitor this aspect in subsequent clinical studies.

PRS060, a single-chain peptide derived from human LCN1, also showed good safety and tolerability in an initial human study.[34] However, it showed respiratory tract pathology in a 13-week toxicology study conducted in nonhuman primates.[35] Although the mechanism underlying this lung injury is unclear, it may be associated with LCN1 derived backbone structure, involved in immune responses and inflammation regulation.[36-38] Elevated LCN1 levels occur under stress from infection or inflammation.[39,40] In fact, PRS060 exhibits structural features similar to LCN1, which may affect removal of harmful lipid molecules, leading to lung injury. In contrast, LQ036 is an Nb with favorable druglike properties, with 4 Nbs already approved by the US Food and Drug Administration.[41-44] Furthermore, our other inhalable Nb targeting thymic stromal lymphopoietin showed no lung injury in a 13-week nonhuman primate Good Laboratory Practice toxicology study (data not shown). Therefore, LQ036 may be a safe inhalable Nb formulation targeting IL-4Rα. Given the safety concern reported with PRS060, a long-term nonclinical toxicology study on LQ036 is promptly required.

DISCLOSURE STATEMENT

This work was funded by grants from the Shanghai Pudong New Area Science and Technology Development Fund Industry-University-Research Special Project (PKX2022-S04), the National Key Research Program (2021YFA0805200), the National Natural Science Foundation of China (32070939, 82030106, and 82270026), the Shanghai Top-Priority Clinical Key Disciplines Construction Project (2017ZZ02013), the Shanghai Municipal Key Clinical Specialty (shslczdzk02201), and the Academic Mentorship for Scientific Research Cadre Project (AMSCP-22-05).

Disclosure of potential conflict of interest: The authors declare that they have no relevant conflicts of interest.

We thank the staff members of the Large-scale Protein Preparation System at the National Facility for Protein Science in Shanghai, Shanghai Advanced Research Institute, Chinese Academy of Sciences, China, for providing technical support and assistance in data collection and analysis, and staff members of beamline BL02U1 and BL19U1 at Shanghai Synchrotron Radiation Facility, China, for data collection.

Clinical implications: Owing to its elevated specificity and affinity, coupled with favorable attributes in terms of efficacy, pharmacokinetics, safety, and tissue distribution, the inhalable LQ036 has advanced to phase IIa clinical trial.

REFERENCES

1. Dalby R, Suman J. Inhalation therapy: technological milestones in asthma treatment. Adv Drug Deliv Rev 2003;55:779-91.
2. Roche N, Aggarwal B, Boucot I, Mittal L, Martin A, Chrystyn H. The impact of inhaler technique on clinical outcomes in adolescents and adults with asthma: a systematic review. Respir Med 2022;202:106949.
3. Ibrahim M, Verma R, Garcia-Contreras L. Inhalation drug delivery devices: technology update. Med Devices (Auckl) 2015;8:131-9.
4. Brusselle GG, Koppelman GH. Biologic therapies for severe asthma. N Engl J Med 2022;386:157-71.
5. McGregor MC, Krings JG, Nair P, Castro M. Role of biologics in asthma. Am J Respir Crit Care Med 2019;199:433-45.
6. Tan R, Liew MF, Lim HF, Leung BP, Wong WSF. Promises and challenges of biologics for severe asthma. Biochem Pharmacol 2020;179:114012.
7. Witt A, Douglass JA, Harun NS. Overview of recent advancements in asthma management. Intern Med J 2022;52:1478-87.
8. Bousquet J, Chiron R, Humbert M. Biologics in asthma: difficulties and drawbacks. Expert Opin Biol Ther 2008;8:1921-8.
9. Steinke JW, Borish L. Th2 cytokines and asthma. Interleukin-4: its role in the pathogenesis of asthma, and targeting it for asthma treatment with interleukin-4 receptor antagonists. Respir Res 2001;2:66-70.
10. Parulekar AD, Kao CC, Diamant Z, Hanania NA. Targeting the interleukin-4 and interleukin-13 pathways in severe asthma: current knowledge and future needs. Curr Opin Pulm Med 2018;24:50-5.
11. Coverstone AM, Seibold MA, Peters MC. Diagnosis and management of T2-high asthma. J Allergy Clin Immunol Pract 2020;8:442-50.
12. Kotsimbos TC, Ghaffar O, Minshall EM, Humbert M, Durham SR, Pfister R, et al. Expression of the IL-4 receptor alpha-subunit is increased in bronchial biopsy specimens from atopic and nonatopic asthmatic subjects. J Allergy Clin Immunol 1998;102:859-66.

13. Dall'Acqua WF, Kiener PA, Wu H. Properties of human IgG1s engineered for enhanced binding to the neonatal Fc receptor (FcRn). J Biol Chem 2006;281:23514-24.
14. Anselmo AC, Gokarn Y, Mitragotri S. Non-invasive delivery strategies for biologics. Nat Rev Drug Discov 2019;18:19-40.
15. Ibrahim M, Wallace I, Ghazvini S, Manetz S, Cordoba-Rodriguez R, Patel SM. Protein aggregates in inhaled biologics: challenges and considerations. J Pharm Sci 2023;112:1341-4.
16. Muyldermans S. Applications of nanobodies. Annu Rev Anim Biosci 2021;9:401-21.
17. Van Heeke G, Allosery K, De Brabandere V, De Smedt T, Detalle L, de Fougerolles A. Nanobodies as inhaled biotherapeutics for lung diseases. Pharmacol Ther 2017;169:47-56.
18. Kunz P, Zinner K, Mucke N, Bartoschik T, Muyldermans S, Hoheisel JD. The structural basis of nanobody unfolding reversibility and thermoresistance. Sci Rep 2018;8:7934.
19. Chen Q, Zhou Y, Yu J, Liu W, Li F, Xian M, et al. An efficient constitutive expression system for Anti-CEACAM5 nanobody production in the yeast *Pichia pastoris*. Protein Expr Purif 2019;155:43-7.
20. Frohlich E, Salar-Behzadi S. Oral inhalation for delivery of proteins and peptides to the lungs. Eur J Pharm Biopharm 2021;163:198-211.
21. Gai J, Ma L, Li G, Zhu M, Qiao P, Li X, et al. A potent neutralizing nanobody against SARS-CoV-2 with inhaled delivery potential. MedComm (2020) 2021;2:101-13.
22. Detalle L, Stohr T, Palomo C, Piedra PA, Gilbert BE, Mas V, et al. Generation and characterization of ALX-0171, a potent novel therapeutic nanobody for the treatment of respiratory syncytial virus infection. Antimicrob Agents Chemother 2016;60:6-13.
23. Cunningham S, Piedra PA, Martinon-Torres F, Szymanski H, Brackeva B, Dombrecht E, et al. Nebulised ALX-0171 for respiratory syncytial virus lower respiratory tract infection in hospitalised children: a double-blind, randomised, placebo-controlled, phase 2b trial. Lancet Respir Med 2021;9:21-32.
24. Möbus L, Rodriguez E, Harder I, Stölzl D, Boraczynski N, Gerdes S, et al. Atopic dermatitis displays stable and dynamic skin transcriptome signatures. J Allergy Clin Immunol 2021;147:213-23.
25. Hamilton JD, Suárez-Farinas M, Dhingra N, Cardinale I, Li X, Kostic A, et al. Dupilumab improves the molecular signature in skin of patients with moderate-to-severe atopic dermatitis. J Allergy Clin Immunol 2014;134:1293-300.
26. Pelaia C, Heffler E, Crimi C, Maglio A, Vatrella A, Pelaia G, et al. Interleukins 4 and 13 in asthma: key pathophysiologic cytokines and druggable molecular targets. Front Pharmacol 2022;13:851940.
27. Pelaia C, Paoletti G, Puggioni F, Racca F, Pelaia G, Canonica GW, et al. Interleukin-5 in the pathophysiology of severe asthma. Front Physiol 2019;10:1514.
28. Rosenberg HF, Phipps S, Foster PS. Eosinophil trafficking in allergy and asthma. J Allergy Clin Immunol 2007;119:1303-10.
29. Nagata M, Nakagome K, Soma T. Mechanisms of eosinophilic inflammation. Asia Pacific Allergy 2020;10:e14.
30. Matschiner G, Fitzgerald MF, Moebius U, Hohlbaum AM, Gille H, Jensen K, et al. Elarekibep (PRS-060/AZD1402), a new class of inhaled Anticalin medicine targeting IL-4Ra for type 2 endotype asthma. J Allergy Clin Immunol 2023;151:966-75.
31. Castro M, Corren J, Pavord ID, Maspero J, Wenzel S, Rabe KF, et al. Dupilumab efficacy and safety in moderate-to-severe uncontrolled asthma. N Engl J Med 2018;378:2486-96.
32. Pieris Pharmaceuticals, Inc. Pieris Pharmaceuticals Announces Successful Completion of Safety Milestone and Initiation of Efficacy Portion of Phase 2a Trial of PRS-060/AZD1402. Boston, MA: Accesswire; 2022. Available at: https://www.accesswire.com/680583/Pieris-Pharmaceuticals-Announces-Successful-Completion-of-Safety-Milestone-and-Initiation-of-Efficacy-Portion-of-Phase-2a-Trial-of-PRS-060AZD1402. Accessed January 3, 2022.
33. Lochhead JJ, Kumar NN, Nehra G, Stenslik MJ, Bradley LH, Thorne RG. Intranasal drug delivery to the brain. In: de Lange ECM, Hammarlund-Udenaes M, Thorne RG, editorsDrug delivery to the brain: physiological concepts, methodologies and approaches. 2nd ed. Cham, Switzerland: Springer; 2022. pp. 461-500.
34. Bruns I, Fitzgerald M, Pardali K, Gardiner P, Keeling D, Axelsson L, et al. First-in-human data for the inhaled IL-4Rα antagonist AZD1402/PRS-060 reveals a promising clinical profile for the treatment of asthma. Am J Respir Crit Care Med 2019;199:A7476.
35. Pieris Pharmaceuticals, Inc. Pieris Pharmaceuticals announces AstraZeneca discontinuation of phase 2a trial of elarekibep (PRS-060/AZD1402) due to new non-clinical safety findings from 13-week toxicology study. Boston, MA: Accesswire; 2023. Available at: https://www.accesswire.com/762604/Pieris-Pharmaceuticals-Announces-AstraZeneca-Discontinuation-of-Phase-2a-Trial-of-Elarekibep-PRS-060AZD1402-Due-to-New-Non-Clinical-Safety-Findings-From-13-week-Toxicology-Study. Accessed June 21, 2023.
36. Dartt DA. Tear lipocalin: structure and function. Ocul Surf 2011;9:126-38.
37. Saaren-Seppala H, Jauhiainen M, Tervo TM, Redl B, Kinnunen PK, Holopainen JM. Interaction of purified tear lipocalin with lipid membranes. Invest Ophthalmol Vis Sci 2005;46:3649-56.
38. Wojnar P, Dirnhofer S, Ladurner P, Berger P, Redl B. Human lipocalin-1, a physiological scavenger of lipophilic compounds, is produced by corticotrophs of the pituitary gland. J Histochem Cytochem 2002;50:433-5.
39. McReynolds S, Vanderlinden L, Stevens J, Hansen K, Schoolcraft WB, Katz-Jaffe MG. Lipocalin-1: a potential marker for noninvasive aneuploidy screening. Fertil Steril 2011;95:2631-3.
40. Wang XR, Li YP, Gao S, Xia W, Gao K, Kong QH, et al. Increased serum levels of lipocalin-1 and -2 in patients with stable chronic obstructive pulmonary disease. Int J Chron Obstruct Pulmon Dis 2014;9:543-9.
41. Duggan S. Caplacizumab: first global approval. Drugs 2018;78:1639-42.
42. Tanaka Y. Ozoralizumab: first Nanobody therapeutic for rheumatoid arthritis. Expert Opin Biol Ther 2023;23:579-87.
43. Markham A. Envafolimab: first approval. Drugs 2022;82:235-40.
44. Fowler NH, Dickinson M, Dreyling M, Martinez-Lopez J, Kolstad A, Butler J, et al. Tisagenlecleucel in adult relapsed or refractory follicular lymphoma: the phase 2 ELARA trial. Nat Med 2022;28:325-32.